A Self-Powered Rectifier-Less Synchronized Switch Harvesting on Inductor Interface Circuit for Piezoelectric Energy Harvesting

Xiudeng Wang, *Student Member, IEEE*, Yinshui Xia, *Member, IEEE*, Ge Shi, Huakang Xia, Zhidong Chen, Yidie Ye, *Member, IEEE*, and Zhangming Zhu

***Abstract*—In this article, a rectifier-less synchronized switch harvesting on inductor (ReL-SSHI) interface circuit for piezoelectric energy harvesting is presented. The proposed circuit works in two different modes: at the positive peak of the open-circuit voltage of the piezoelectric transducer (PZT), the switch in series with the load is turned ON, and is operated in the series synchronized switch harvesting on inductor mode; at the negative peak of the open-circuit voltage of the PZT, the switch in parallel with the load is turned ON, and is operated in voltage synchronous inversion mode. The ReL-SSHI circuit does not need a rectifier bridge so that the power loss of the circuit is reduced, and hence the piezoelectric energy harvesting efficiency of the circuit is improved. Theoretical analysis and simulation verify the effectiveness of the ReL-SSHI circuit.**

***Index Terms*—Piezoelectric energy harvesting, piezoelectric transducer (PZT), rectifier-less, self-powered, series synchronized switch harvesting on inductor (S-SSHI).**

I. Introduction

HARVESTING ambient energy to power wireless sensor network nodes has become one of the effective methods to solve the problem of limited power supply life. Piezoelectric energy harvester (PEH) can harvest energy from environmental vibration sources, which is a promising technology. According to the electromechanical coupling characteristic of the piezoelectric element, electricity can be generated when it is strained. Because the deformation of the piezoelectric patch is alternating, the generated current is also alternating [1]. However, common electronic equipment requires a dc power supply. Hence, an interface circuit with rectification and voltage regulation function is required.

The simplest interface circuit is the full-bridge rectifier (FBR) circuit. Many researchers have made their efforts in the optimization of the FBR circuit and even implemented the integrated circuit in CMOS [2], [3]. However, the harvesting efficiency is still low because of the existence of a parasitic capacitor in the piezoelectric element and a phase difference between the voltage and current resulting in reactive power in such a circuit [4], [5].

It is hard for the FBR to efficiently harvest piezoelectric energy from a low electromechanical coupling PEH. Therefore, the parallel synchronized switch harvesting on inductor (P-SSHI), the synchronous electric charge extraction (SECE), and the series synchronized switch harvesting on inductor (S-SSHI) circuits were proposed for effectively harvesting piezoelectric energy from low electromechanical coupling PEH [6]–[8]. Subsequently, Liang *et al.* [1] proposed a self-powered synchronized switch harvesting on inductor (SP-SSHI) circuit and compared to the FBR circuit, the maximum output power can be increased by 200%. Shi *et al.* [9] proposed a self-powered efficient synchronous electric charge extraction circuit and the maximum output power of this circuit can reach three times that of the FBR. Furthermore, a low-phase lag peak detector was proposed and applied to the SECE circuit. The maximum output power of the circuit can reach 3.56 times that of the FBR circuit [5]. Shao *et al.* [10] proposed a highly efficient P-SSHI rectifier for piezoelectric energy harvesting and the experimental results showed that the proposed circuit can provide 5.8 times boost in harvested energy compared to the FBR circuit. Sanchez *et al.* [11] proposed an autonomous piezoelectric energy harvesting system based on the P-SSHI technique, which can harvest energy from periodic and shocking excitation and extract up to 6.81 times more power compared with the ideal FBR circuit. Eltamaly *et al.* [12] proposed an SP-SSHI circuit, which has a 10% efficiency increase compared to the circuit in [1]. Chen *et al.* [13] proposed an improved self-powered P-SSHI circuit, the maximum output power of the circuit can reach 3.6 times that of the FBR circuit. Liang *et al.* [14] proposed a new interface circuit called the parallel synchronized triple bias-flip (P-S3BF)

Manuscript received July 9, 2020; revised October 11, 2020 and December 6, 2020; accepted January 15, 2021. Date of publication January 19, 2021; date of current version May 5, 2021. This work was supported in part by the National Natural Science Foundation of China under Grants U1709218, 61971389, 61801253, and 61601429, in part by the Natural Science Foundation of Zhejiang Province under Grants LZ20F010006 and LY20F010003, in part by the Natural Science Foundation of Ningbo under Grants 2018A610091 and 2019A610113, and in part by the K. C. Wong Magna Fund in Ningbo University. Recommended for publication by Associate Editor M. A. E. Andersen. *(Corresponding author: Yinshui Xia.)*

Xiudeng Wang, Yinshui Xia, Huakang Xia, Zhidong Chen, and Yidie Ye are with the Faculty of Electrical Engineering and Computer Science, Ningbo University, Ningbo 315211, China (e-mail: 1611082572@nbu.edu.cn; xiayinshui@nbu.edu.cn; xiahuakang@nbu.edu.cn; 1701082016@nbu.edu.cn; yeyidie@nbu.edu.cn).

Ge Shi is with the College of Mechanical and Electrical Engineering, China Jiliang University, Hangzhou 310018, China (e-mail: shige@cjlu.edu.cn).

Zhangming Zhu is with the School of Microelectronics, Xidian University, Xi'an 710071, China (e-mail: zhangmingzhu@xidian.edu.cn).

Color versions of one or more figures in this article are available at https://doi.org/10.1109/TPEL.2021.3052573.

Digital Object Identifier 10.1109/TPEL.2021.3052573

for further boosting the harvesting capability. From their experimental results, the maximum output power of the circuit can reach 3.88 times that of the FBR circuit. The SECE and SSHI use inductors for high efficiency, which results in a large volume of the PEH. In order to realize miniaturized harvesters, circuits based on synchronized switch harvesting on capacitors (SSHC) have been studied. Du *et al.* [15] proposed an inductor less bias-flip rectifier for the PEH, which shows a 9.7× performance improvement compared with the FBR. Chen *et al.* [16] proposed a split-phase flipping-capacitor rectifier with capacitor reuse for input power adaptation, and its maximum efficiency can reach 9.3 times that of the FBR.

According to the summary of Brenes *et al.*, [17] it can be known that each interface has the maximum output power under the optimal electrical tuning conditions. This maximum power point (MPP) voltage changes when the vibrations characteristics change, and therefore MPP tracking (MPPT) is needed [18]. Shi *et al.* [19] proposed a quasi-MPPT system based on FBR with open-circuit voltage sampling and bidirectional dc–dc voltage conversion. Moreover, active bridge rectifiers with multidimensional MPPT have been proposed in [20], which has a good performance of MPPT without requiring the high-frequency sampling and elaboration of the harvester current or voltage.

Although these advanced contributions have significantly improved the efficiency of the PEH, the typical SECE and SSHI have low efficiency in low-voltage harvesting [21]. Especially, when the vibration is weak, the power consumed by the rectifier diodes may even exceed the power obtained by the load. To solve this issue, Cai *et al.* [22] proposed an interface with fully autonomous conjugate impedance matching, which does not require a diode rectifier so that power consumption can be reduced and low-voltage piezoelectric energy can be harvested. Du *et al.* [23] proposed an SSHI interface, which can extract energy from a weak vibration excitation source. Although these solutions can harvest low-voltage piezoelectric energy, they increase the complexity of the circuit and require complex active control circuits. In addition, the SSHI with magnetic rectifier is also used to harvest low-voltage piezoelectric energy while it requires a larger volume transformer with two primary windings and one secondary winding [24], [25].

In this article, a rectifier-less synchronized switch harvesting on inductor (ReL-SSHI) structure is proposed, and the implementation of a self-powered ReL-SSHI circuit is described in detail. The proposed ReL-SSHI structure mainly includes an inductor and two switches, which greatly simplifies the circuit, reduces the number of components, and hence decreases power consumption. Moreover, it can efficiently harvest low-voltage piezoelectric energy.

In Section II, the S-SSHI circuit is briefly analyzed, and the circuit topology of the proposed ReL-SSHI is introduced. In Section III, the specific implementation of the ReL-SSHI circuit is presented, and its working principle is explained. In Section IV, the simulation analysis of the ReL-SSHI circuit is presented. In Section V, the experimental results are provided. Finally, Section VI concludes the article.

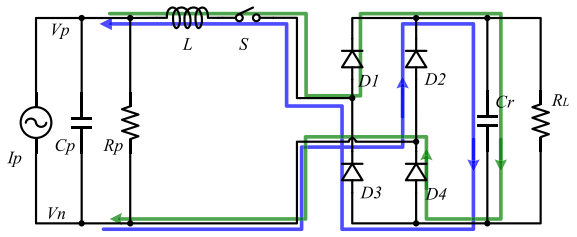

Fig. 1. Schematic of the S-SSHI interface.

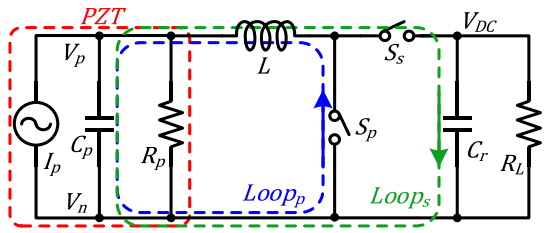

Fig. 2. Topological structure of the ReL-SSHI.

II. S-SSHI and ReL-SSHI

A. S-SSHI Circuit

The S-SSHI is a typical energy harvesting circuit for PEH, as shown in Fig. 1. According to the working principle of the S-SSHI, when the open-circuit voltage of the piezoelectric transducer (PZT) reaches the peak, the switch is turned ON, the capacitors C_p, C_r, and the inductor L form an LC resonant loop. As known, two diodes in the loop will consume part of the energy extracted from the PZT, which will reduce the quality factor of the LC loop.

The energy loss of the LC resonant loop can be expressed as

$$\Delta E_{\mathrm{LC}} = \int_0^{\pi\sqrt{\mathrm{LC}}} (2V_D + V_S)\, I_{\mathrm{LC}} + r_{\mathrm{ESR}} I_{\mathrm{LC}}^2 dt. \quad (1)$$

V_D is the conduction voltage drop of the diode, V_S is the conduction voltage drop of the switch, r_{ESR} is the equivalent series internal resistance of the inductor, and the I_{LC} is the current of the LC resonant loop. From (1), if the energy consuming components in the LC resonant loop can be reduced, the power consumption of the circuit can be saved, which is advantageous for improving the efficiency of the LC resonance.

B. ReL-SSHI Circuit

The proposed ReL-SSHI interface structure is shown in Fig. 2.

Compared with the S-SSHI, the ReL-SSHI eliminates the rectifier bridge by adding a switch. Its working principle is as follows. When V_p reaches the peak, the switch S_s is turned ON, the capacitors C_p, C_r, and the inductor L form an LC resonant loop. After 1/2 LC resonance period, part of the energy accumulated on C_p is transferred to the C_r, and the remaining energy reversely charges C_p so that the voltage of C_p is reversed, which is the same as the operation principle of the S-SSHI. When V_n reaches the peak, the switch S_p is turned ON, then the capacitor C_p and the inductor L form the LC resonant loop. After 1/2 LC resonance

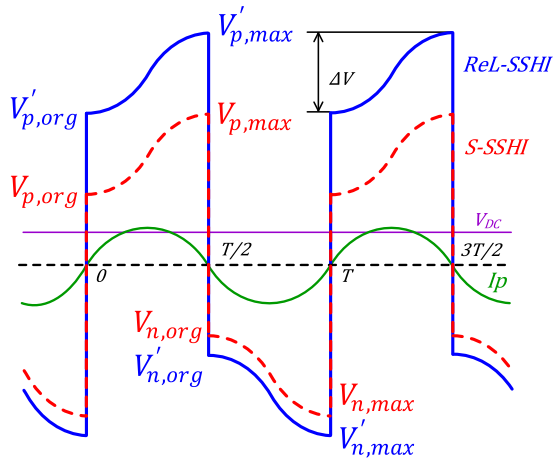

Fig. 3. Open-circuit voltage of the PZT in the ReL-SSHI and S-SSHI.

period, the voltage of the capacitor C_p is inverted. From Fig. 2, it can be seen that the LC resonant loop in the ReL-SSHI circuit has no additional energy-consuming components such as diodes, which is beneficial for the ReL-SSHI to achieve more efficient LC resonance.

Define Q_s and Q_p as the electrical quality factor of the LC resonant Loop_s and Loop_p in Fig. 2, respectively. The inversion factors of the corresponding LC loop can be expressed as

$$\begin{cases} \gamma_s = e^{-\pi/2Q_s}, \ 1 > \gamma_s > 0 \\ \gamma_p = e^{-\pi/2Q_p}, \ 1 > \gamma_p > 0. \end{cases} \tag{2}$$

Fig. 3 shows the open-circuit voltage waveforms of the PZT in the S-SSHI and ReL-SSHI circuits. As illustrated, the ReL-SSHI and S-SSHI have similar waveforms, except that the S-SSHI is symmetric on the horizontal axis, whereas the positive voltage of the ReL-SSHI is significantly higher than the negative voltage. During a vibration cycle, the ReL-SSHI operates in the S-SSHI mode for most of the time and works in voltage synchronous inversion mode only during the 1/2 LC resonance period of the rising edge.

According to the description in [8], it can be known that

$$\begin{cases} V'_{n,\mathrm{org}} + V_{DC} = \gamma_s \left(V'_{p,\max} - V_{\mathrm{DC}}\right) \\ V'_{p,\mathrm{org}} = \gamma_p \, V'_{n,\max} \end{cases} \tag{3}$$

where V_{DC} represents the output voltage of the ReL-SSHI circuit, and $V'_{n,\mathrm{org}}$, $V'_{p,\max}$, $V'_{p,\mathrm{org}}$, and $V'_{n,\max}$ correspond to the voltage indication symbols in Fig. 3.

The charge amount that the current source I_p charges capacitor C_p in a half cycle is

$$Q_e = \int_0^{T/2} I_p dt. \tag{4}$$

Therefore, the variation amount of open-circuit voltage of the PZT in a half cycle can be expressed as

$$\begin{aligned} \Delta V = V'_{p,\max} - V'_{p,\mathrm{org}} &= V'_{n,\max} - V'_{n,\mathrm{org}} = V_{p,\max} \\ - V_{p,\mathrm{org}} &= V_{n,\max} - V_{n,\mathrm{org}} = \frac{Q_e}{C_p} = \frac{2\alpha U_M}{C_p}. \end{aligned} \tag{5}$$

α and U_M are, respectively, the force factor and displacement amplitude of the piezoelectric patch. When the maximum displacement amplitude of the piezoelectric cantilever remains unchanged, the Q_e and ΔV in the electrical domain will keep unchanged.

The following can be derived from the above equation

$$V_{n,\mathrm{org}} = \frac{\Delta V \gamma_s (1+\gamma_p) - V_{DC}(1+\gamma_s)}{1-\gamma_s\gamma_p}. \tag{6}$$

According to the working principle of the ReL-SSHI, the harvested energy is transmitted to the load once per cycle. The energy transmitted to the load in the half LC resonant period of the falling edge is

$$E_{\mathrm{ReL}} = \int_0^{T/2} V_{\mathrm{DC}} \cdot I dt = V_{\mathrm{DC}} C_p \left(V'_{p,\max} + V'_{n,\mathrm{org}}\right) = \frac{2\pi V_{\mathrm{DC}}^2}{\omega R_L}. \tag{7}$$

It can be obtained as follows:

$$\begin{aligned} V'_{p,\max} + V'_{n,org} &= \frac{\Delta V \gamma_s (1+\gamma_p)(\gamma_s+1)}{\gamma_s(1-\gamma_s\gamma_p)} \\ &+ \frac{V_{DC}\left((1+\gamma_s)(1-\gamma_s\gamma_p) - (1+\gamma_s)^2\right)}{\gamma_s(1-\gamma_s\gamma_p)}. \end{aligned} \tag{8}$$

It can be further obtained as follows:

$$V_{\mathrm{DC}} = \frac{\Delta V \gamma_s (1+\gamma_p)(\gamma_s+1)}{\frac{2\pi\gamma_s(1-\gamma_s\gamma_p)}{R_L\omega C_p} - (1+\gamma_s)(1-\gamma_s\gamma_p) - (1+\gamma_s)^2}. \tag{9}$$

The average harvested power expression is given as follows:

$$P = \frac{V_{\mathrm{DC}}^2}{R_L}. \tag{10}$$

For a constant displacement amplitude, the average harvested power reaches the maximum value, $P_{\mathrm{ReL-SSHI,max}}$, which is given in (11) under an optimal equivalent load resistance $R_{\mathrm{ReL-SSHI,opt}}$ as shown in (12)

$$\begin{aligned} P_{\mathrm{ReL-SSHI,max}} &= \frac{\Delta V^2 \omega C_p}{8\pi} \frac{(1+\gamma_p)(1+\gamma_s)}{1-\gamma_s\gamma_p} \\ &= \frac{f\alpha^2 U_M^2}{C_p} \frac{(1+\gamma_p)(1+\gamma_s)}{1-\gamma_s\gamma_p} \end{aligned} \tag{11}$$

$$R_{\mathrm{ReL-SSHI,opt}} = \frac{1-\gamma_s\gamma_p}{fC_p(1+\gamma_p)(1+\gamma_s)}. \tag{12}$$

According to (11), the maximum output power of the ReL-SSHI is proportional to the vibration frequency, the square of displacement amplitude, and inversely proportional to the clamped capacitance of the piezoelectric patch. In addition, it is closely related to the inversion (electrical quality) factor of the LC loop of the ReL-SSHI circuit.

The output power of the ReL-SSHI can also be expressed as

$$\begin{aligned} P_{\mathrm{ReL-SSHI}} &= fV_{\mathrm{DC}}C_p\left(V'_{p,\max} + V'_{n,\mathrm{org}}\right) \\ &= \frac{fC_pV_{\mathrm{DC}}(\Delta V - V_{\mathrm{DC}})(1+\gamma_s)(1+\gamma_p)}{1-\gamma_s\gamma_p}. \end{aligned} \tag{13}$$

Then, the equation is differentiated to $V_{\rm dc}$, when its derivative is zero, the optimal load voltage can be obtained:

$$V_{\rm DC\_ReL,opt} = \frac{\Delta V}{2} = V_{\rm OC,org} \tag{14}$$

where $V_{\rm OC,\ org}$ is the original open-circuit voltage of the PZT. In the actual circuit, if the power loss of the circuit is considered, the optimal load voltage will be lower than $V_{\rm OC,org}$.

From the research of Lefeuvre *et al.* [8], it is known that the maximum output power, optimal load resistance, and optimal load voltage of the S-SSHI are

$$P_{\rm S-SSHI,max} = \frac{f\alpha^2 U_M^2}{C_p}\frac{1+\gamma_s}{1-\gamma_s} \tag{15}$$

$$R_{\rm S-SSHI,opt} = \frac{1}{4fC_p}\frac{1-\gamma_s}{1+\gamma_s} \tag{16}$$

$$V_{\rm DC\_S,opt} = \frac{\Delta V}{4} = \frac{V_{\rm OC,org}}{2}. \tag{17}$$

If the conduction voltage drop of the rectifier diode is considered, there is

$$V_{\rm DC\_S,opt} = \frac{V_{\rm OC,org}}{2} - 2V_D \tag{18}$$

where, V_D is the conduction voltage drop of the rectifier diode.

Therefore, the minimum $V_{\rm OC,org}$ of the S-SSHI should be higher than $2V_D$, and the MPPT can be achieved only when the minimum $V_{\rm OC,\ org}$ is higher than $4V_D$. However, from (14), as long as the minimum $V_{\rm OC,\ org}$ of the ReL-SSHI is higher than zero, piezoelectric energy can be harvested (the inductor and switches losses are not considered).

It should be noted that the maximum power described in (11) and (15) is the energy that the circuit can theoretically harvest. In other words, it represents the maximum power that the PEH can convert mechanical energy into electrical energy. Therefore, even though the S-SSHI and ReL-SSHI use the same inductor, the LC loop of the S-SSHI contains two diodes and has a lower inversion factor, which will result in the theoretical maximum harvestable power of the S-SSHI being lower than that of the ReL-SSHI.

III. Implementation of the ReL-SSHI

The detailed implementation of the self-powered ReL-SSHI circuit is shown in Fig. 4. Except for the load and the PZT, only one inductor, one capacitor, and four transistors (two PNPs, two NPNs) are used.

As can be seen from Fig. 4, the self-powered ReL-SSHI circuit requires fewer devices than the previously proposed self-powered piezoelectric energy harvesting interface circuits. The devices required in each circuit are listed in Table I.

In order to explain the working principle of the ReL-SSHI circuit in Fig. 4, one work cycle is divided into six phases based on the open-circuit voltage variation of the PZT as shown in Fig. 5.

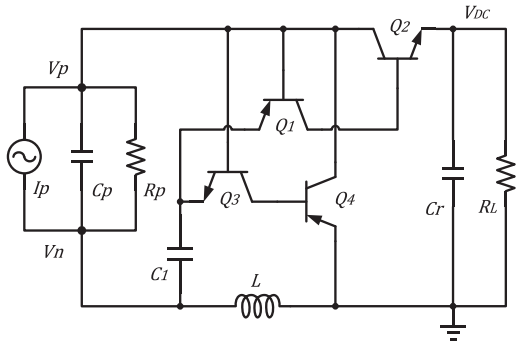

Fig. 4. Self-powered ReL-SSHI circuit.

TABLE I
Devices Used in the Circuits

	[1]	[9]	[12]	[13]	This work
Transistors	4	4	4	4	**4**
MOS FETs	0	2	0	0	**0**
Capacitors	2	2	2	2	**1**
Inductors	1	1	1	1	**1**
Diodes	8	7	4	12	**0**
Resistors	2	2	0	4	**0**

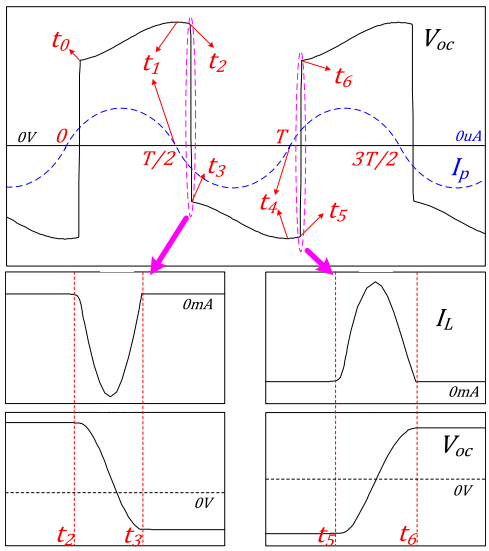

Fig. 5. Typical waveforms of the ReL-SSHI circuit in Fig. 4.

A. First Natural Charging Phase ($t_0 < t < t_1$)

During this phase, capacitors C_1, C_p are parallel and the flow directions of all currents are shown in Fig. 6(a).

The open-circuit voltage of the PZT can be expressed as

$$V_{\rm oc}\ (t) = V_{\rm oc,t0} + \frac{\int_{t0}^{t} I_p dt}{C_p}\ (t_0 \le t \le t_1)\ . \tag{19}$$

Suppose I_p is expressed as

$$I_p = A\sin(wt)\,. \tag{20}$$

The open-circuit voltage of the PZT reaches the maximum value of the positive half-cycle at the time t_1, which can be

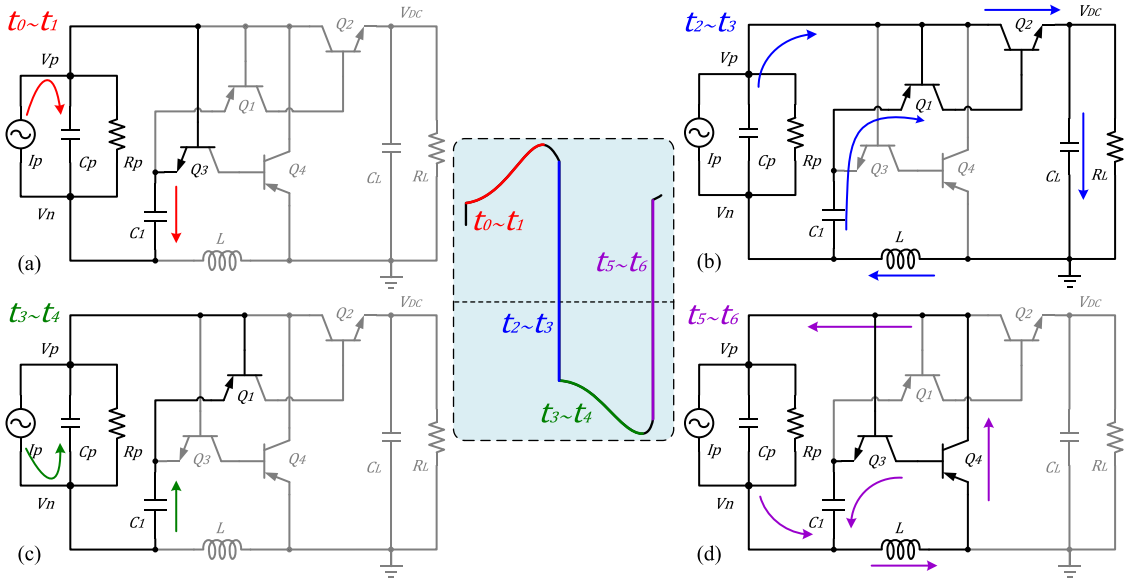

Fig. 6. Flow directions of currents in (a) first natural charging ($t_0 < t < t_1$), (b) first voltage inversion ($t_2 < t < t_3$), (c) second natural charging ($t_3 < t < t_4$), (d) second voltage inversion ($t_5 < t < t_6$).

expressed as

$$V_{\mathrm{oc},p\max} = V_{\mathrm{oc},t1} = V_{\mathrm{oc},t0} + \frac{\int_{t0}^{t1} A\sin(wt)\,dt}{C_p}$$
$$= V_{\mathrm{oc},t0} + \frac{\int_{0}^{\frac{T}{2}} A\sin(wt)\,dt}{C_p} - 2V_{\mathrm{be}}$$
$$= V_{oc,t0} + \frac{2A}{wC_p} - 2V_{\mathrm{be}} \tag{21}$$

where V_{be} is the base-emitter threshold voltage of the transistor. The reason why $2V_{\mathrm{be}}$ is subtracted from the equation is that there is a phase lag between the switching action time (t_2) and the PZT's open-circuit voltage peak time (t_1), which is caused by the base-emitter threshold voltage of the transistor. A detailed description will be given.

At this point, the open-circuit voltage of the PZT reaches the peak, and the energy accumulated in C_p reaches a maximum:

$$E_{Cp} = \frac{1}{2} C_p V_{oc,p\max}^2 \tag{22}$$

At the same time, the voltage of the capacitor C_1 also reaches its maximum value:

$$V_{c1,p\max} = V_{oc,p\max} - V_{\mathrm{be}}. \tag{23}$$

B. First Current Reversion Phase ($t_1 < t < t_2$)

At the time t_1, I_p crosses over zero, the current begins to reverse charge C_p, and the charge stored in C_p begins to be released, so that the open-circuit voltage of the PZT begins to decrease gradually. However, the charge stored in the capacitor C_1 cannot be released because there is no loop so that the voltage of C_1 remains unchanged.

At the time t_2, the open-circuit voltage of the PZT is lower than the voltage of C_1 by a threshold voltage of the PNP transistor Q_1, which causes Q_1 to be turned ON and the charge accumulated on C_1 begins to be released.

At this instant, the open-circuit voltage of the PZT can be expressed as

$$V_{oc,t2} = V_{c1,p\max} - V_{be} = V_{oc,p\max} - 2V_{\mathrm{be}}. \tag{24}$$

Then, the phase lag between the switching action time and the peak time of the open-circuit voltage of the PZT can be expressed as

$$\theta = \cos^{-1}\left(\frac{V_{\mathrm{oc},p\max} - 2V_{\mathrm{be}}}{V_{\mathrm{oc},p\max}}\right). \tag{25}$$

C. First Voltage Inversion Phase ($t_2 < t < t_3$)

After transistor Q_1 is turned ON, Q_2 is also turned ON. The circuit immediately enters the first voltage inversion phase. The capacitors C_1, C_p , C_r and the inductor L form an LC resonant loop, as shown in Fig. 6(b). After half LC resonant period, the charge accumulated in capacitors C_1 and C_p is transferred to the load through the LC loop, while C_p is charged reversely, causing the voltage of C_p to flip. The working principle during this phase is the same as that of the S-SSHI circuit. However, there are no redundant energy-consuming components in the LC loop of the ReL-SSHI circuit, which reduces the power loss of the circuit and also means that the LC resonance loop has higher efficiency.

For the LC loop, the main energy loss of the circuit is caused by the switching transistor Q_2 and the equivalent series resistance (ESR) of the inductor L. Therefore, the power loss of the first voltage inversion phase can be expressed as

$$\Delta E_{\mathrm{LC},1st} = \int_0^{\pi\sqrt{\mathrm{LC}}} V_{ce} I_L + r_{\mathrm{ESR}} I_L^2 dt. \tag{26}$$

I_L represents the current of the inductor, which represents the current of the LC resonant loop in the equation. $V_{\rm ce}$ is the collector–emitter voltage of the transistor, and $r_{\rm ESR}$ is the ESR of the inductor. Compared with (1), it can be found that the power lost at LC resonant loop by the ReL-SSHI circuit is lower than the S-SSHI circuit.

Assuming that the electrical quality factor of the LC loop is Q'_s, its inversion factor can be expressed as

$$\gamma'_s = e^{-\pi/2Q'_s},\ 0 < \gamma'_s < 1. \tag{27}$$

For the first inversion, from t_2 to t_3, the relation between $V_{{\rm oc},t2}$ and $V_{{\rm oc},t3}$ can be obtained as

$$V_{{\rm oc},t3} + (V_{\rm DC} + V_{\rm ce}) = \gamma'_s\ [V_{{\rm oc},t2} - (V_{\rm DC} + V_{\rm ce})]\ . \tag{28}$$

Here, both $V_{{\rm oc},t2}$ and $V_{{\rm oc},t3}$ refer to the absolute value of the open-circuit voltage of the PZT at times t_2 and t_3, $V_{\rm ce}$ is the collector–emitter voltage of the transistor Q_2.

D. Second Natural Charging Phase ($t_3 < t < t_4$)

During this period, it works the same as the first natural charging phase. The current source I_p charges capacitor C_p from the V_n terminal, while capacitor C_1 is charged through the base-emitter of transistor Q_1 , as shown in Fig. 6(c).

E. Second Current Reversion Phase ($t_4 < t < t_5$)

At the instant t_4, I_p crosses zero, the current begins to charge C_p from the V_p terminal. This phase works in the same way as the first current reversion phase until the open-circuit voltage of the PZT is lower than the voltage of C_1 by a transistor threshold voltage $V_{\rm be}$, transistors Q_3 and Q_4 are turned ON, and the circuit proceeds to the next phase.

F. Second Voltage Inversion Phase ($t_5 < t < t_6$)

After transistor Q_4 is turned ON, the circuit immediately enters the second voltage inversion phase. The capacitors C_1, C_p, and the inductor L form an LC resonant loop, as shown in Fig. 6(d). After half LC resonant period, the charge accumulated on the capacitor C_p is transferred from the V_n terminal to the V_p terminal, and at the same time, the open-circuit voltage of the PZT is inverted.

Assuming that the electrical quality factor of the LC loop is Q'_p, its inversion factor can be expressed as

$$\gamma'_p = e^{-\pi/2Q'_p},\ 0 < \gamma'_p < 1. \tag{29}$$

For the second inversion, from t_5 to t_6, the relation between $V_{{\rm oc},t5}$ and $V_{{\rm oc},t6}$ can be obtained as

$$V_{{\rm oc},t6} + V_{\rm ec} = \gamma'_p\ (V_{{\rm oc},t5} - V_{\rm ec})\,. \tag{30}$$

Here, both $V_{{\rm oc},t5}$ and $V_{{\rm oc},t6}$ refer to the absolute value of the open-circuit voltage of the PZT at times t_5 and t_6, $V_{\rm ec}$ is the emitter–collector voltage of the transistor Q_4.

It is important to note that an appropriate capacitance should be chosen for the capacitor C_1 in the peak detector. The capacitance of C_1 is mainly related to the dc gain β of the transistors and the parasitic capacitance C_p of the PZT. Since the charge accumulated in C_1 is released through the base of the switching transistor, it meets

$$C_1 > \frac{1}{\beta} C_p. \tag{31}$$

If the capacitance of C_1 is small, it may cause the following problems: the energy in C_p will has not been fully extracted before the switching transistor is disconnected; the ON-resistance of the switching transistor is large. However, if the capacitance of C_1 is too large, the energy transferred from I_p to C_p will be reduced since the C_1 and C_p are connected in parallel; the power consumption of the peak detector is increased.

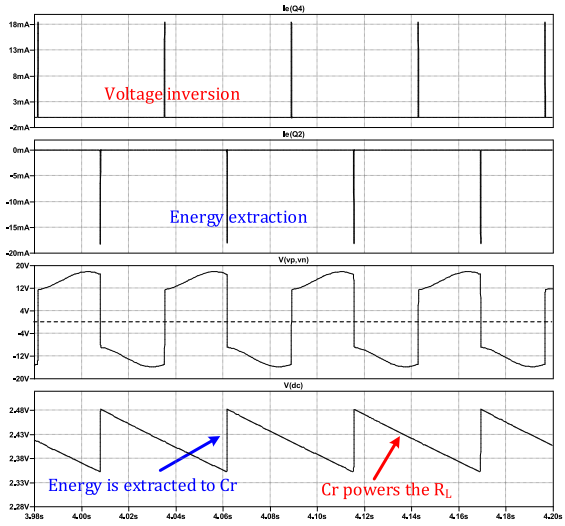

Fig. 7. Voltage and current simulation waveform of the ReL-SSHI.

IV. Simulation Analysis

In order to verify the above analysis of the ReL-SSHI circuit, the simulation of the circuit is carried out ($f = 18.6\,{\rm Hz}$, $I_p = 60\,\mu{\rm A}$, $R_p = 1\,{\rm M\Omega}$, $C_p = 100\,{\rm nF}$, $C_1 = 1\,{\rm nF}$, $C_r = 20\,\mu{\rm F}$, $L = 50\,{\rm mH}$ at $r_{\rm ESR} = 100\,\Omega$, and $R_L = 50\,{\rm k\Omega}$). Fig. 7 shows the current and voltage waveforms obtained by simulation, which are derived directly from the simulation software LTspice.

As can be seen from the figure, the open-circuit voltage waveform of the PZT is similar to that of the S-SSHI, but it is not symmetric on the x-axis. The absolute value of $V_{p,\max}$ is larger than that of $V_{n,\max}$. At the falling edge of the open-circuit voltage of the PZT, transistor Q_2 generates a current pulse, at which point the PZT, the load capacitor C_r, and the inductor L resonate, and part of the energy of the PZT is transferred to the load. Therefore, the output voltage will rise rapidly. The energy extracted from the PZT can be expressed as

$$P_E = P_H + P_L = \frac{1}{2} C_p \left(V_1^2 - V_2^2\right) \tag{32}$$

where P_H and P_L represent the energy harvested at the load and the energy loss by the circuit, respectively.

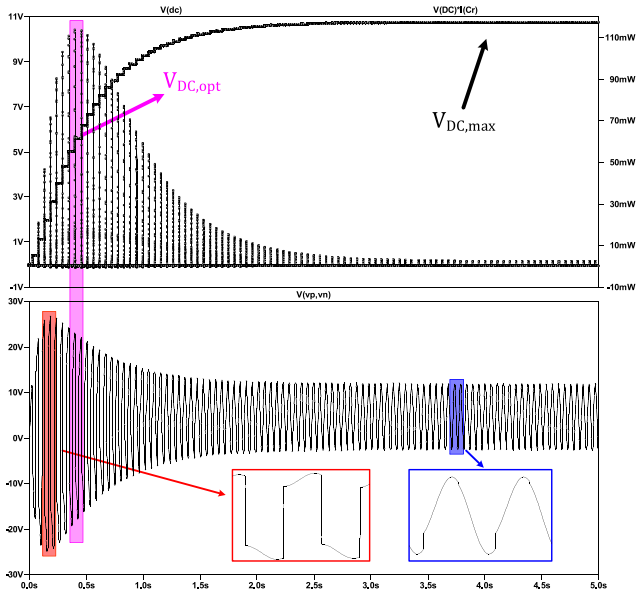

Fig. 8. Comparison of output power under different V_{DC}.

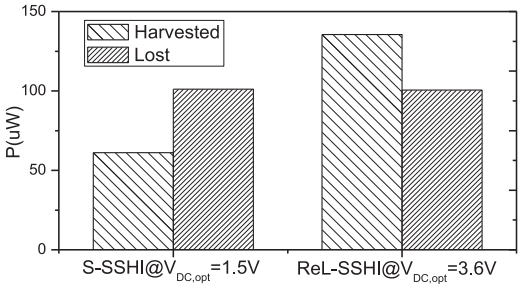

Fig. 9. Harvested power and lost power at the maximum power point.

At the rising edge of the open-circuit voltage of the PZT, transistor Q_4 generates a current pulse, at which point the PZT and the inductor L resonate, and the open-circuit voltage of the PZT is inverted. Therefore, there is no energy transferred to the load during the rising edge.

Fig. 8 shows the simulated waveform of the self-powered ReL-SSHI circuit when the load is a capacitor ($f = 18.6$ Hz, $I_p = 80$ μA, $R_p = 1$ MΩ, $C_p = 100$ nF, $C_1 = 1$ nF, $C_r = 5$ μF, and L = 50 mH at $R_{\mathrm{ESR}} = 100$ Ω). According to the working principle of the ReL-SSHI, the circuit transfers energy to the load once in each vibration period. Hence, the power graph of the load capacitor is a pulse waveform. It can be seen that as the load voltage increases, the amplitude of the power pulse of the load capacitor and the open-circuit voltage of the ReL-SSHI both increase first and then decrease. In addition, according to the simulation data, the optimal load voltage $V_{\mathrm{dc,opt}}$ is slightly smaller than the original open-circuit voltage of the PZT equivalent circuit, which is about half of the maximum output voltage $V_{\mathrm{dc,max}}$. Therefore, the ReL-SSHI can efficiently harvest piezoelectric energy depending on a suitable load voltage, which is consistent with the description in (14).

The harvested power and lost power of the circuit at the MPP for the S-SSHI and the ReL-SSHI are compared in Fig. 9.

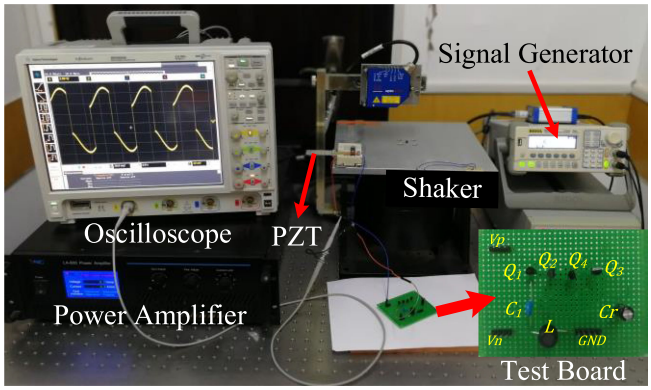

Fig. 10. Experimental setup.

Although two circuits use the same peak detector and inductor with equal power loss, the power harvested by the S-SSHI is significantly lower than that of the ReL-SSHI, because the conversion efficiency of the S-SSHI is lower than that of the ReL-SSHI. Combined with the previous theoretical analysis, it can be known that the diodes in the S-SSHI reduce the inversion factor of the LC loop, which not only reduce the conversion efficiency of the circuit but also reduce the maximum harvestable power of the S-SSHI circuit.

V. Experiment Analysis

In order to verify the above theoretical and simulation analysis, the experimental platform is set up as shown in Fig. 10. The experimental system mainly includes a function signal generator, an oscilloscope, the PZT, a power amplifier, a shaker, and the self-powered ReL-SSHI interface circuit. One end of the PZT is fixed on the shaker, the function signal generator drives the shaker through the power amplifier to increase the driving ability. The vibration amplitude and frequency of the shaker can be adjusted by the signal generator. The PNP and NPN transistors used in the circuit are 2N3906 and 2N3904, respectively. The capacitor C_1 is a 1 nF high-voltage ceramic capacitor, and the load capacitor C_r is a 220 μF electrolytic capacitor. The inductor is a 50 mH I-shaped inductor with an internal resistance of 102 Ω. The piezoelectric patch chosen is the PPA-1014 from MIDE, which has a parasitic capacitance of 41 nF. One end of the piezoelectric patch is fixed on the shaker, while the other end is tied to a metal block. The resonance frequency of the cantilever beam is inversely proportional to the mass and distance of the metal block. Adjusting the output power of the power amplifier can control the vibration amplitude of the shaker, and adjusting the frequency of the signal generator can change the vibration frequency of the shaker. When the output power of the power amplifier remains unchanged and the cantilever beam device is fixed, the resonance frequency of the cantilever beam can be found by adjusting the frequency of the shaker. The open-circuit voltage of the piezoelectric patch at the resonance frequency is the largest, which means that the output power of the piezoelectric patch is the largest at this frequency. The original resonant frequency of the experimental device is

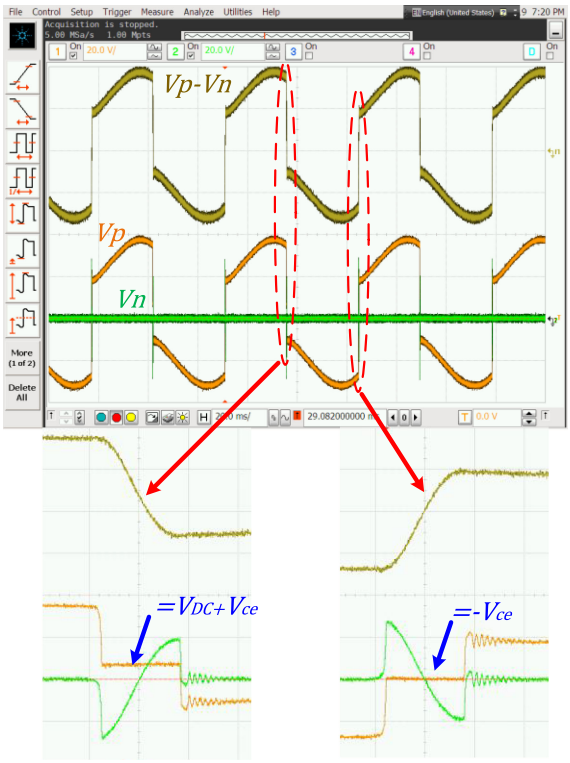

Fig. 11. Experimental waveforms.

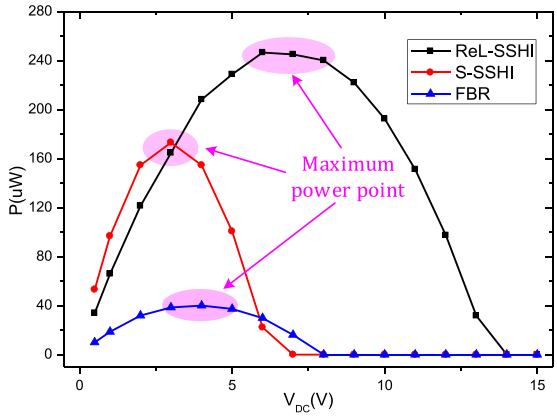

Fig. 12. Harvested power under different V_{DC}.

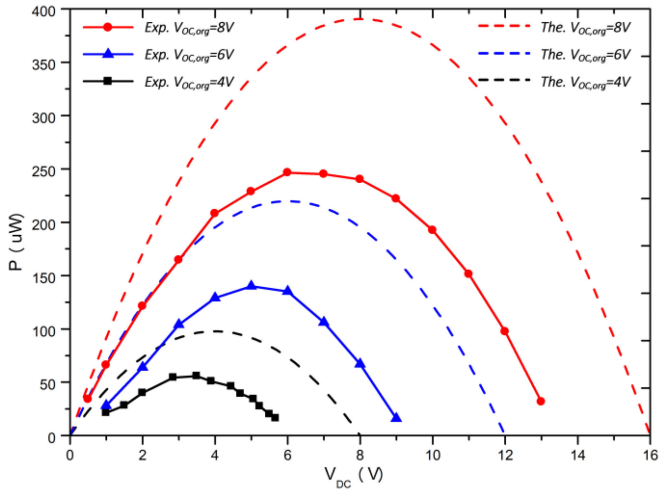

Fig. 13. Harvested power under different excitation amplitudes (The.: theory; Exp.: experiment).

about 18.4 Hz, when the ReL-SSHI circuit is connected, the resonant frequency becomes about 18.6 Hz.

Fig. 11 shows that the voltage waveforms are measured by the oscilloscope and the amplified waveforms at the rising and falling edges. The open-circuit voltage waveform of the PZT is similar to the S-SSHI circuit, but the open circuit voltage is not symmetric about the x-axis, which is consistent with the theoretical analysis and simulation results. At the falling edge, the PZT, inductor, and load form the LC resonant loop, V_p is located at the positive terminal of the transistor Q_2 and the load. Hence, V_p is equal to the output voltage V_{DC} plus the turn-ON voltage drop V_{ce} of the switching transistor Q_2. At the rising edge, the inductor and the PZT form the LC resonant loop, and V_p is at the collector of transistor Q_4 , so V_p is equal to $-V_{\mathrm{ce}}$.

Fig. 12 shows the harvested power of the ReL-SSHI, S-SSHI, and the FBR under the same vibration condition (the original open-circuit voltage of the piezoelectric patch is about 8 V) with different output voltages. Among them, the ReL-SSHI and S-SSHI used the same peak detector (including two PNP transistors, two NPN transistors, a ceramic capacitor, and an equivalent inductor, and the diodes used in the FBR and S-SSHI circuit are 1N4148). It can be seen from the figure that when the output voltage is less than 3 V, the S-SSHI performs well, and when the output voltage is higher than 3 V, the ReL-SSHI performs the best. From (11) and (15), it can be found that the theoretically maximum extractable power of the ReL-SSHI and S-SSHI is equal (regardless of the circuit loss). However, as can be seen from Fig. 12, the maximum output power of the S-SSHI is less than that of the ReL-SSHI from the experimental test. This is that the rectifier bridge in the S-SSHI reduces the inversion factor of the LC loop, which not only decreases the conversion efficiency of the circuit but also reduces the maximum harvestable power of the circuit. In contrast, the ReL-SSHI has a higher maximum harvestable power and higher conversion efficiency due to its high inversion factor.

From the figure, it can be seen that the optimal output voltage of the S-SSHI is less than that of the FBR, and is about half of the optimal output voltage of the ReL-SSHI, which is consistent with the theoretical analysis of (14), (17), and (18).

Fig. 13 shows the output power curve under different excitation amplitudes. The theoretical output power in the figure is calculated according to (13), which represents the electric power generated by the PZT, and it does not include the energy loss of the circuit and caused by the delay of the switching action. It can be seen from the figure that the optimal load voltage and maximum output power of the experiment are smaller than that of the ideal circuit, which is consistent with the previous analysis. The following conclusion can be drawn from the figure: output voltage range and the optimal load voltage are approximately linearly related to the vibration amplitude; the maximum power

TABLE II
PERFORMANCE COMPARISON

Circuits	TIE2012[1]	TPEL2015[10]	TCAS2018[5]	JSSC2020[16]	TPEL2019[14]	TPEL2019[13]	This Work
PZT	N/A	V22B	YiBoP8-1	PPA-1021	PZT-5A	N/A	**PPA-1014**
C_p (nF)	33.74	18	220	22	28.42	68.2	**41**
Scheme type	S-SSHI	P-SSHI	SECE	SSHC	P-S3BF	P-SSHI	**ReL-SSHI**
Self-powered	YES	NO	YES	NO	NO	YES	**YES**
Inductor	47mH	940uH	1mH	N/A	47mH	50mH	**50mH**
$P_{out,max}/P_{FBR,max}$	3	5.8	3.56	9.3	3.88	3.6	**5.9**
Frequency (Hz)	30	225	42	200	24.9	50	**18.6**
$V_{OC,org}$ (V)	5-25	V_{OC}=2.4-3.28*	1.5-5	V_{OC}=1.4V*	15	V_{OC}=5*	**4-8**

**V_{OC} is the open-circuit voltage of the PEH connected to the rectifier, N/A = Not applicable.

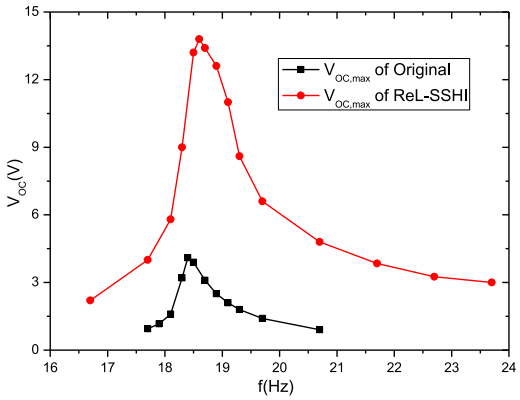

Fig. 14. Maximum open-circuit voltage at different vibration frequencies.

harvested by the circuit is linearly related to the square of the vibration amplitude. These characteristics are consistent with the description of (11) and (14).

According to the experiments, the lowest open-circuit voltage corresponding to harvested piezoelectric energy by the S-SSHI is about 1.6 V. However, under the same conditions, the lowest open-circuit voltage by the ReL-SSHI is about 0.9 V. If an accurate peak detector is used to reduce the delay of the switching timing, theoretically, the ReL-SSHI can harvest piezoelectric energy at a lower voltage.

Fig. 14 shows the maximum original open-circuit voltage of the piezoelectric patch and the maximum open-circuit voltage when the piezoelectric patch is connected to the ReL-SSHI circuit under different vibration frequencies. As can be seen from the figure, the resonance frequency of the cantilever beam rises slightly, and the open-circuit voltage of the piezoelectric patch has a significant increase compared to the original state. In addition, when the ReL-SSHI circuit is connected, the 3 dB bandwidth is increased by about 70%, which is beneficial for harvesting piezoelectric energy.

Table II lists the comparison results for piezoelectric energy harvesting circuits published in recent years, including the SECE, S-SSHI, P-SSHI, and the proposed ReL-SSHI circuits. Compared with the circuits proposed in [1], [13], [14], using a similar inductance value, the harvesting efficiencies of these circuits are significantly lower than that of the ReL-SSHI circuit proposed in this article. In addition, the P-S3BF circuit proposed in [14] has a complicated control module so that an external power supply is required. The P-SSHI circuit proposed in [10] has a high harvesting efficiency with a small inductor while it also needs an external power supply to start the circuit. When the output voltage reaches 1.8 V, the circuit can be adjusted to the self-powered mode, however, from the experimental data, the harvesting efficiency drops significantly. The SECE circuit proposed in [5] reduces the phase lag of the switching action instant and it can maintain high efficiency in a wide load range, but the circuit power consumption still limits its energy harvesting efficiency. The SSHC circuit in [16] can achieve efficient piezoelectric energy harvesting without using inductors. However, its complex control module is unfavorable for achieving cold self-starting or requires an inefficient passive circuit to assist in achieving cold self-starting.

VI. CONCLUSION

To obtain efficient energy harvesting interface circuits, in this article, an ReL-SSHI interface was proposed. Compared with the conventional S-SSHI circuit, the proposed ReL-SSHI circuit needs fewer devices and hence potentially is of lower power consumption and lower cost. Theoretical analysis, simulation, and experimental results confirm that the ReL-SSHI circuit has the advantages of high energy harvesting efficiency.

REFERENCES

[1] J. Liang and W. Liao, "Improved design and analysis of self-powered synchronized switch interface circuit for piezoelectric energy harvesting systems," *IEEE Trans. Ind. Electron.*, vol. 59, no. 4, pp. 1950–1960, Apr. 2012.

[2] Y. Li *et al.*, "An ultra-low-voltage self-powered energy harvesting rectifier with digital switch control," *IEICE Electron. Exp.*, vol. 12, no. 3, pp. 20140921–20140921, 2015.

[3] A. L. F. Stein and H. F. Hofmann, "Autonomous wideband piezoelectric energy harvesting utilizing a resonant inverter," *IEEE Trans. Power Electron.*, vol. 32, no. 8, pp. 6178–6187, Aug. 2017.

[4] D. A. Sanchez, J. Leicht, F. Hagedorn, E. Jodka, E. Fazel, and Y. Manoli, "A parallel-SSHI rectifier for piezoelectric energy harvesting of periodic and shock excitations," *IEEE J. Solid-State Circuits*, vol. 51, no. 12, pp. 2867–2879, Dec. 2016.

[5] G. Shi, Y. Xia, X. Wang, L. Qian, Y. Ye, and Q. Li, "An efficient self-powered piezoelectric energy harvesting CMOS interface circuit based on synchronous charge extraction technique," *IEEE Trans. Circuits Syst. I: Regular Papers*, vol. 65, no. 2, pp. 804–817, Feb. 2018.
[6] E. Lefeuvre and C. Richard, "High-performance piezoelectric vibration energy reclamation," in *Proc. Int. Soc. Opt. Eng.*, 2004, pp. 379–387.
[7] E. Lefeuvre *et al.*, "Piezoelectric energy harvesting device optimization by synchronous charge extraction," *J. Intell. Mater. Syst. Struct.*, vol. 16, no. 10, pp. 865–876, 2005.
[8] E. Lefeuvre *et al.*, "A comparison between several vibration-powered piezoelectric generators for standalone systems," *Sensors Actuators A Phys.*, vol. 126, no. 2, pp. 405–416, 2006.
[9] G. Shi *et al.*, "An efficient self-powered synchronous electric charge extraction interface circuit for piezoelectric energy harvesting systems," *J. Intell. Mater. Syst. Struct.*, vol. 27, no. 16, pp. 2160–2178, 2016.
[10] S. Lu and F. Boussaid, "A highly efficient P-SSHI rectifier for piezoelectric energy harvesting," *IEEE Trans. Power Electron.*, vol. 30, no. 10, pp. 5364–5369, Oct. 2015.
[11] D. A. Sanchez, J. Leicht, F. Hagedorn, E. Jodka, E. Fazel, and Y. Manoli, "A parallel-SSHI rectifier for piezoelectric energy harvesting of periodic and shock excitations," *IEEE J. Solid-State Circuits*, vol. 51, no. 12, pp. 2867–2879, Dec. 2016.
[12] A. M. Eltamaly and K. E. Addoweesh, "A novel self-power SSHI circuit for piezoelectric energy harvester," *IEEE Trans. Power Electron.*, vol. 32, no. 10, pp. 7663–7673, Oct. 2017.
[13] Z. Chen, J. He, J. Liu, and Y. Xiong, "Switching delay in self-powered nonlinear piezoelectric vibration energy harvesting circuit: Mechanism, effects and solution," *IEEE Trans. Power Electron.*, vol. 34, no. 3, pp. 2427–2440, Mar. 2019.
[14] J. Liang, Y. Zhao, and K. Zhao, "Synchronized triple bias-flip interface circuit for piezoelectric energy harvesting enhancement," *IEEE Trans. Power Electron.*, vol. 34, no. 1, pp. 275–286, Jan. 2019.
[15] S. Du and A. A. Seshia, "An inductorless bias-flip rectifier for piezoelectric energy harvesting," *IEEE J. Solid-State Circuits*, vol. 52, no. 10, pp. 2746–2757, Oct. 2017.
[16] Z. Chen, M. K. Law, P. I. Mak, X. Zeng, and R. P. Martins, "Piezoelectric energy-harvesting interface using split-phase flipping-capacitor rectifier with capacitor reuse for input power adaptation," *IEEE J. Solid-State Circuits*, vol. 55, no. 8, pp. 2106–2117, Aug. 2020.
[17] A. Brenes, A. Morel, J. Juillard, and E. Lefeuvre, "Maximum power point of piezoelectric energy harvesters: A review of optimality condition for electrical tuning," *Smart Mater. Struct.*, vol. 29, no. 3, Dec. 2020, Art. no. 033001.
[18] L. Costanzo, A. L. Schiavo, and M. Vitelli, "Power extracted from piezoelectric harvesters driven by non-sinusoidal vibrations," *IEEE Trans. Circuits Syst.*, vol. 66, no. 3, pp. 1291–1303, Mar. 2019.
[19] G. Shi *et al.*, "An efficient power management circuit based on quasi maximum power point tracking with bidirectional intermittent adjustment for vibration energy harvesting," *IEEE Trans. Power Electron.*, vol. 34, no. 10, pp. 9671–9685, Oct. 2019.
[20] L. Costanzo, A. Lo Schiavo, and M. Vitelli, "Active interface for piezoelectric harvesters based on multi-variable maximum power point tracking," *IEEE Trans. Circuits Syst. I: Regular Papers*, vol. 67, no. 7, pp. 2503–2515, Jul. 2020.
[21] D. Guyomar and M. Lallart, "Recent progress in piezoelectric conversion and energy harvesting using nonlinear electronic interfaces and issues in small scale implementation," *Micromachines*, vol. 2, no. 2, pp. 274–294, 2011.
[22] Y. Cai and Y. Manoli, "A piezoelectric energy-harvesting interface circuit with fully autonomous conjugate impedance matching, 156% extended bandwidth, and 0.38μW power consumption," in *Proc. IEEE Int. Solid-State Circuits Conf.*, 2018, pp. 148–150.
[23] S. Du, Y. Jia, C. Do, and A. A. Seshia, "An efficient SSHI interface with increased input range for piezoelectric energy harvesting under variable conditions," *IEEE J. Solid-State Circuits*, vol. 51, no. 11, pp. 2729–2742, Nov. 2016.
[24] L. Garbuio, M. Lallart, D. Guyomar, C. Richard, and D. Audigier, "Mechanical energy harvester with ultralow threshold rectification based on SSHI nonlinear technique," *IEEE Trans. Ind. Electron.*, vol. 56, no. 4, pp. 1048–1056, Apr. 2009.
[25] M. Lallart *et al.*, "High efficiency, wide load bandwidth piezoelectric energy scavenging by a hybrid nonlinear approach," *Sensors Actuators A-Phys.*, vol. 165, no. 2, pp. 294–302, 2011.

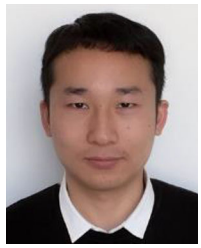

Xiudeng Wang (Student Member, IEEE) received the B.S. degree in communication engineering and the M.S. degree in electronic circuit and systems in 2016 and 2019, respectively, from Ningbo University, Ningbo, China, where he is currently working toward the Ph.D. degree in electronic science and technology.

His research interests include energy harvesting technique, sensors and measuring technology, ultralow power integrated circuits design, as well as embedded system.

Yinshui Xia (Member, IEEE) received the B.S. degree in physics and the M.S. degree in electronic engineering from Hangzhou University, Zhejiang, China, in 1984 and 1991, respectively, and the Ph.D. degree in electronic engineering from Edinburgh Napier University, Edinburgh, U.K., in 2003.

He was a Visiting Scholar with King's College London, London, U.K., in 1999, and then joined Edinburgh Napier University, Edinburgh, U.K., as a Research Assistant and Enterprise Fellow from 2000 to 2005. He is currently a Professor with the Faculty of Electrical Engineering and Computer Science, Ningbo University, Ningbo, China. His research interests include low-power digital circuit design, logic synthesis and optimization, and system on chip design.

Ge Shi received the B.E. degree in electrical engineering and automation and the M.S. degree in detection technology and automation from China Jiliang University, Zhejiang, China, in 2004 and 2010, respectively, and the Ph.D. degree in micronano information system from Ningbo University, Ningbo, China, in 2018.

He is a Senior Experimentalist with China Jiliang University, Hangzhou, China. His research interests include energy harvesting systems, sensors and measuring technology, low-power integrated circuits design, as well as embedded system.

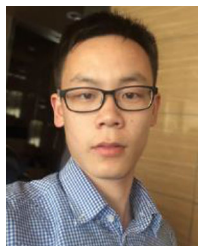

Huakang Xia received the B.S. degree in aircraft design and engineering and the Ph.D. degree in instrument science and technology from Nanjing University of Aeronautics and Astronautics, Nanjing, China, in 2012 and 2017, respectively.

He is currently a Lecturer with the Faculty of Electrical Engineering and Computer Science, Ningbo University, Ningbo, China. His research interests include energy harvesting systems, intelligent monitoring technology, and IoT devices.

Zhidong Chen received the B.S. degree in electronic and information engineering and the M.S. degree in electronic circuit and system from Hangzhou Dianzi University, Zhejiang, China, in 2011 and 2014, respectively. He is currently working toward the Ph.D. degree with the Faculty of Electrical Engineering and Computer Science, Ningbo University, Ningbo, China.

He is a Lecturer with Zhejiang Business Technology Institute, Ningbo, China. His research interests include energy harvesting systems, sensors, and measuring technologies.

Yidie Ye (Member, IEEE) received the B.S., M.S., and Ph.D. degrees in microelectronics from Zhejiang University, Hangzhou, China, in 2007, 2010, and 2012, respectively.

She is currently a Lecturer with the Faculty of Electrical Engineering and Computer Science, Ningbo University, Ningbo, China. Her research interests include low-power circuit design and optimization.

Zhangming Zhu received the B.S., M.S., and Ph.D. degrees in microelectronics from Xidian University, Xi'an, China, in 2000, 2003, and 2004, respectively.

Since 2009, he has been a Professor with the School of Microelectronics, Xidian University. He has authored/coauthored more than 70 articles in IEEE journal. His research interests include analog, mixed-signal, power, and RF-integrated circuits and systems.

Prof. Zhu currently serves as an Associate Editor for the IEEE TRANSACTIONS ON CIRCUITS AND SYSTEMS—II: EXPRESS BRIEFS.